Available online at www.sciencedirect.com
ScienceDirect
Magnetic Resonance Imaging 29 (2011) 620–629
MAGNETIC RESONANCE IMAGING

Deconvolution with simple extrapolation for improved cerebral blood flow measurement in dynamic susceptibility contrast magnetic resonance imaging during acute ischemic stroke

Matthew Ethan MacDonald[a,b,e,f], Michael Richard Smith[a,b,c], Richard Frayne[a,b,c,d,e,f,*]

[a]Biomedical Engineering, University of Calgary, Alberta, Canada T2N 1N4
[b]Electrical and Computer Engineering, University of Calgary, Alberta, Canada T2N 1N4
[c]Radiology, University of Calgary, Alberta, Canada T2N 2T9
[d]Clinical Neurosciences, University of Calgary, Alberta, Canada T2N 2T9
[e]Hotchkiss Brain Institute, University of Calgary, Alberta, Canada T2N 2T9
[f]Seaman Family MR Research Centre, Foothills Medical Centre, Alberta Health Services, Calgary, Alberta, Canada T2N 2T9

Received 3 October 2010; revised 2 February 2011; accepted 20 February 2011

Abstract

Magnetic resonance (MR) perfusion imaging is a clinical technique for measuring brain blood flow parameters during stroke and other ischemic events. Ischemia in brain tissue can be difficult to accurately measure or visualize when using MR-derived cerebral blood flow (CBF) maps. The deconvolution techniques used to estimate flow can introduce a mean transit time-dependent bias following application of noise stabilization techniques. The underestimation of the CBF values, greatest in normal tissues, causes a decrease in the image contrast observed in CBF maps between normally perfused and ischemic tissues; resulting in ischemic areas becoming less conspicuous. Through application of the proposed simple extrapolation technique, CBF biases are reduced when missing high-frequency signal components in the MR data removed during deconvolution noise stabilization are restored. The extrapolation approach was compared with other methods and showed a statistically significant increase in image contrast in CBF maps between normal and ischemic tissues for white matter ($P<.05$) and performed better than most other methods for gray matter. Receiver operator characteristic curve analysis demonstrated that extrapolated CBF maps better-detected penumbral regions. Extrapolated CBF maps provided more accurate CBF estimates in simulations, suggesting that the approach may provide a better prediction of outcome in the absence of treatment.
© 2011 Elsevier Inc. All rights reserved.

Keywords: Deconvolution; Perfusion–diffusion mismatch; Extrapolation; Tracer kinetics

1. Introduction

Ischemic stroke is a devastating disease that can potentially result in both disability and death. Ischemic stroke occurs when an embolism or thrombus occludes an artery that feeds blood to a region of brain tissue. The blockage restricts blood flow to this region, and if left untreated, the affected tissue may become infarcted [1]. With prompt treatment, some of the ischemic, but not yet infarcted, tissue may be salvaged. In the proposed and idealized model, this ischemic but not infarcted tissue is referred to as the "tissue at risk" or the penumbral region [2]. The concept of tissue penumbra suggests that accurate knowledge of cerebral blood flow (CBF) is of importance in assessing tissue affected by a blockage that may be still salvageable with proper treatment.

Magnetic resonance (MR) perfusion-weighted imaging (PWI) can estimate CBF in the brain. Using fast MR imaging, changes in image signal intensity are sampled as a tracer (contrast agent) passes through the brain's circulation system. From these temporally resolved image data, important blood flow parameters including time to peak (TTP), CBF, cerebral blood volume (CBV) and mean transit time (MTT) can be obtained [3]. When combined with diffusion-weighted imaging (DWI), PWI has been demonstrated to predict tissue outcome in acute ischemic stroke cases. The MR perfusion–

* Corresponding author. Seaman Family MR Research Centre, Foothills Medical Centre, Calgary, Alberta, Canada T2N 2T9. Tel.: +1 403 944 8321; fax: +1 403 270 7907.
E-mail address: rfrayne@ucalgary.ca (R. Frayne).

0730-725X/$ – see front matter © 2011 Elsevier Inc. All rights reserved.
doi:10.1016/j.mri.2011.02.024

diffusion mismatch theory [4] is a conceptual model that allows penumbral tissue to be determined soon after the onset of stroke (i.e., within 3–6 h) by comparing abnormalities on DWI to PWI deficits. Hyperintense lesions on diffusion images are assumed to be infarcted tissue that is not likely to recover with treatment [5]. Perfusion imaging shows the tissue affected by the blockage as having reduced flow, which may become infarcted if normal flow is not reestablished. By using DWI and PWI for stroke assessment, an estimate of the volume of salvageable tissue can be obtained, providing valuable information for determining the appropriate course of patient treatment.

In PWI studies, the cerebral vascular system is modeled as a linear system of concentration functions [6–10]. The MR signal intensity time signals are converted to concentration time series signals; then the concentration function from a feeding artery, $C_a(t)$, the tissue concentration function, $C_T(t)$, and the flow-scaled system response, CBF·$R(t)$ can be related by

$$C_T(t) = \mathrm{CBF} \cdot \mathrm{R}(t) \otimes C_a(t), \quad (1)$$

where ⊗ denotes the convolution operator, and CBF·$R(t)$ is the flow-scaled mass density function response bounded between CBF and 0 (i.e., max($R(t)$)=1; max(CBF·$R(t)$)=CBF). Eq. 1 may be used to solve for CBF in a variety of ways, but most quantitative methods require signal deconvolution. Deconvolution is an ill-posed problem and requires regularization in the presence of noise. The method of regularization (and the associated parameters) used when performing deconvolution can change resulting CBF values and distort the perceived patient prognosis. All deconvolution methods reduce the high-frequency components of the residue function.

Deconvolution can be performed either in the time domain, through matrix manipulation or in the frequency domain, by dividing corresponding spectral components [6,7]. Both approaches are theoretically equivalent [8]. Both are also ill-posed problems, becoming unstable due to high-frequency noise components after the deconvolution operation. Noise reduction is achieved either implicitly (in the case of regularizing a matrix inversion in the time-domain approaches) or explicitly (low-pass filtering of spectral components in the frequency-domain approaches) [8]. Both regularization and low-pass filtering are key steps to reduce high-frequency noise, but come with the penalty of also reducing high-frequency components of the desired signals, artificially creating an erroneous CBF dependence on tissue MTT. Short MTT signals (healthy tissue) are broadest in the frequency domain and are thus more heavily filtered [11]. Conversely, longer MTT tissues (such as in stroke-affected tissue) produce time signals with less energy at higher frequencies and are less affected by filtering. With this systematic underestimation of the CBF values from healthy tissue, current deconvolution-based approaches effectively decrease the image contrast between normal and ischemic regions, making stroke-affected regions less conspicuous.

Several research groups have investigated methods for improving this process and providing more robust CBF estimates. Østergaard et al. [6,7] demonstrated how CBF maps could be created by regularizing the deconvolution process. They showed that the optimal thresholding (or filtering) value was a function of the image signal-to-noise ratio (SNR_I). These optimal filtering techniques used the same threshold across the entire image. Later studies by Liu et al. [12] proposed an adaptive filtering scheme that varied the effective threshold and thus allowed more high-frequency energy to be retained. The level of noise filtering by Liu et al. was based on an assessment of the concentration time-course SNR ratio (SNR_C). Ridge-based regularization techniques have also been implemented, such as Tikhonov regularization, which do not remove any information but rather introduces energy across the diagonal of the matrix facilitating its inversion [13]. Introduction of energy across the matrix diagonal can be effective but does not always ensure inversion and can itself result in erroneous values. Frequency-domain signal modeling, such as using least-square fits to Lorentzian functions, has been proposed for estimation of the signal [14]. Model-independent estimation techniques, such as the autoregressive moving average [15] or generalized cross-validation [16], have also been proposed but, in general, are difficult to implement as current image acquisitions have relatively few time points to process and build these elaborate models robustly.

Most commonly used deconvolution-based techniques provide relative CBF estimates due to partial voluming and other sources of error. Cross-calibration [9], a process where the CBF of regions of normal WM is scaled to 22 ml 100 g^{-1} min^{-1}, is nearly always used to provide more physiologically correct flow values in normal tissue. However, scaling to force the underestimated WM CBF value to take the value 22 ml 100 g^{-1} min^{-1}, simultaneously, introduces a systemic overestimation in the CBF for tissues with longer MTT values [16] changing the outline of the penumbra region. Cross-calibration, because the maps are linearly scaled, does not impact the normal-ischemic tissue image contrast in CBF maps.

We expect that the proposed simple extrapolation approach, by attempting to restore the high-frequency components of the filtered flow-scaled residue function, will minimize the MTT-dependent errors and enhance the normal-ischemic image contrast in stroke patients. This will produce a more robust CBF map in perfusion experiments and improve conspicuity between healthy and ischemic tissue. In this work, simulation of perfusion signals was undertaken to find optimal estimators and parameters that can be used for deconvolution in our clinical imaging protocol. CBF was calculated with four common deconvolution methods and with a new extrapolation-based method. Perfusion imaging data sets were collected from 10 ischemic stroke patients and then reconstructed with each of the five methods using the optimized parameters. Statistical analysis was then undertaken to test for the hypothesized change in

image contrast between healthy and ischemic tissues. Finally, an assessment of the ability to predict final tissue state in one untreated patient was performed using receiver operator characteristic (ROC) analysis.

2. Theory

With MR PWI, a four-dimensional data set (a temporal series of images) is collected during the passage of a contrast agent bolus traversing through the brain. Paramagnetic contrast agents, such as gadopentetate dimeglumine, cause a local regional shortening in T_2 and T_2* relaxation times, resulting in a reduction in localized MR image signal intensity. The MR signal intensity functions are converted to concentration functions using well-established relationships [3,6,7] and are modeled with an exponential,

$$S(t) = S_0 e^{-\frac{TE}{k}C(t)}, \tag{2}$$

where S_0 is the baseline MR signal intensity, TE is the echo time, k is the proportionality constant, and $C(t)$ is the contrast agent concentration time function. Inverting Eq. 2 allows the measured MR signal intensity functions to be converted to concentration functions, $C(t) = -k/\mathrm{TE}\ \ln(S(t)/S_0)$.

Four deconvolution methods are compared in this study as they represent benchmarks against which the simple extrapolation approach can be assessed. Three of the methods are time-domain regularization approaches, where a linear system of equations is formulated, $\boldsymbol{C}_\mathrm{T}=\mathrm{CBF}\boldsymbol{C}_\mathrm{a}\mathbf{R}$, and inverted to solve for CBF. $\boldsymbol{C}_\mathrm{T}$ is the contrast concentration in the tissue vector, $\boldsymbol{C}_\mathrm{a}$ is the contrast concentration in a supplying artery (or the arterial input function) matrix, and $\mathbf{R}$ is the tissue residue function vector. The time-domain deconvolution methods require that $\boldsymbol{C}_\mathrm{a}$ be inverted. Regularization of $\boldsymbol{C}_\mathrm{a}$ is required prior to inversion in the presence of noise.

Previously reported methods tend toward the use of time-domain inversion techniques based on singular value decomposition (SVD)-based deconvolution [6,7,9,10,17]. The approaches explored in this study include the block-circulatant SVD (bcSVD) [8,18,19], Tikhonov regularization (sometimes referred to as ridge regularization) [13,20], and Tikhonov SVD (TikhoSVD) [20]. In addition to these time-domain approaches, spectral division (SD) is also used as a benchmark [6–8]. In this approach, the signals are converted to their Fourier domain representations and divided. Each of these methods, and the mechanisms they use to control noise instabilities, are described in more detail in the following sections.

2.1. Block-circulatant SVD

bcSVD has been demonstrated to be superior to the previously implemented standard SVD method by being delay insensitive [18,19]. $\boldsymbol{C}_\mathrm{a}$ is decomposed using SVD into $\mathbf{U}\boldsymbol{\Lambda}\mathbf{V}^\mathrm{T}$, where $\boldsymbol{\Lambda}$ is a diagonal matrix of the eigenvalues, λ_i. The inverse of $\boldsymbol{C}_\mathrm{a}$ can be found by the linear product, $\mathbf{V}$ [diag $(1/\lambda_i)$]$\mathbf{U}^\mathrm{T}$. Eigenvalue thresholding is used by setting to zero all eigenvalues below a particular threshold, P_SVD. Other processing techniques can attempt to smooth the eigenfunction or minimize error in a least-squares sense [20].

2.2. Tikhonov regularization for deconvolution

Deconvolution can also be performed using Tikhonov regularization [13,16], by inverting $\boldsymbol{C}_\mathrm{a}$ in a least-squares minimization sense. A matrix, $\boldsymbol{\Gamma}$, is introduced and is most often chosen as a scaled identity matrix, $\alpha\mathbf{I}$. A pseudo-solution can then be found for the flow-scaled residue function (CBF $\mathbf{R}$) by,

$$\mathrm{CBF}\,\mathbf{R} = \left(C_\mathbf{a}^\mathrm{T}C_\mathbf{a} + \alpha^2\mathbf{I}\right)^{-1}C_\mathbf{a}^\mathrm{T}C_\mathrm{T}. \tag{3}$$

2.3. Tikhonov regularization with SVD

Another implementation of Tikhonov regularization is combined with SVD (these methods are similar but do not result in the same outcome under all conditions). The matrix $\boldsymbol{C}_\mathrm{a}$ is decomposed with SVD into $\mathbf{U}\boldsymbol{\Lambda}\mathbf{V}^\mathrm{T}$, then the inverse of $\boldsymbol{C}_\mathrm{a}$ is found by the linear product of $\mathbf{V}\mathbf{G}\mathbf{U}^\mathrm{T}$, where $\mathbf{G}$ is a diagonal matrix having components, g_i, created from the eigenvalues of $\boldsymbol{\Lambda}$:

$$g_i = \lambda_i / \left(\lambda_i^2 + \alpha^2\right). \tag{4}$$

2.4. SD for deconvolution

In addition to these time-domain formulations, deconvolution can also be performed in the frequency domain with SD. The CBF·$R(f)$ can be found by,

$$\mathrm{CBF}\ \cdot R(f) = \frac{C_\mathrm{T}(f)}{C_\mathrm{a}(f),} \tag{5}$$

where $R(f)$, $C_\mathrm{T}(f)$ and $C_\mathrm{a}(f)$ are the frequency-domain representations of $R(t)$, $C_\mathrm{T}(t)$ and $C_\mathrm{a}(t)$, respectively. Noise causes instability particularly in low-intensity high-frequency components (Fig. 1A). This erratic behavior is a result of $C_\mathrm{a}(f)$ approaching zero and destabilizing the division. In the SD approach, low-pass filtering is often applied to remove the erratic high-frequency components from CBF·$R(f)$. By taking the inverse Fourier transform of the filtered flow-scaled system response (i.e., $w_f(f)$·CBF·$R(f)$), an estimate of CBF can be derived. It has been previously shown that low-pass filtering in the frequency domain is related to P_SVD thresholding in the time domain [8] by way of the applied frequency-domain window function,

$$w(f) = \begin{cases} 1 & |C_\mathrm{a}(f)| > P_\mathrm{SVD}\,|C_\mathrm{a}(f)|_{max} \\ 0 & \ldots \end{cases}, \tag{6}$$

under the assumption that $C_\mathrm{a}(f)$ is monotonically decreasing with f near $|C_\mathrm{a}(f)| = P_\mathrm{SVD}\cdot|C_\mathrm{a}(f)|_\mathrm{max}$. Filtering, like time-domain thresholding, also results in an error with an MTT dependence (Fig. 1B).

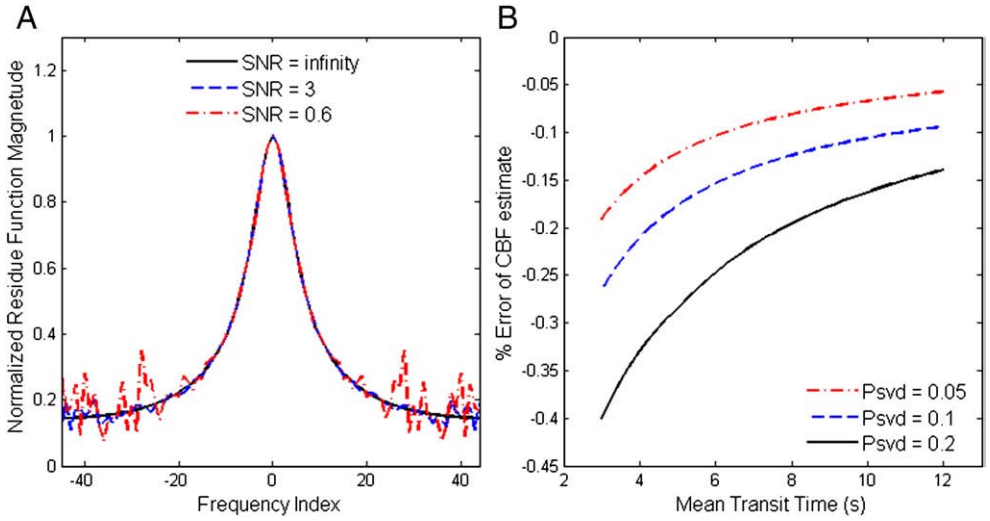

Fig. 1. Simulation results of the residue function and CBF dependence on MTT. (A) The normalized magnitude frequency spectrum of a deconvolved residue function, for no noise and two noise levels. At higher frequencies with noise, the residue function becomes unstable. Noise has been added (Gaussian distribution) to MR signal intensities (SNR=S_0/σ_{SIGNAL}). The MTT was 4.8 s. (B) Noise-free simulations show an increasing error with decreasing MTT and increasing level of P_{SVD} filtering applied. Higher levels of P_{SVD} are typically required to reduce the impact of high-frequency noise. Deconvolution was performed with the Fourier-windowed SD method. The equivalent low-pass filter to a P_{SVD} threshold was used (see Eq 6). Other parameters used in the simulations were as follows: CBV=1.74 ml 100 g^{-1}; ATD=0.1 s; Δt=2 s.

2.5. Extrapolation-based deconvolution

The proposed simple extrapolation method extrapolates from the known complex values, of $R(f)$, to estimate (recover) the high-frequency components of the residue function truncated during the noise stability procedure. To reflect the band-limited nature of the residue function, the $R(f)$ values are set to zero after a defined extent of frequencies (known as the extrapolation length, $L_{EXTRAPOLATE}$; Figs. 2A and B). In principle, this operation could be performed on residue functions obtained from any deconvolution method, but in this study, it will only be applied to residue functions generated by the SD algorithm.

The CBF error changes proportionally to MTT (Fig. 1B), which is related to the signal width in the time domain. The extent of high-frequency extrapolation is set to be inversely proportional to the frequency width of the signal. In order to complete the extrapolation procedure after the initial $R(f)$ estimate has been obtained, an estimate of MTT ($MTT_{ESTIMATE}$) is required. Since the width of $R(f)$ in the frequency domain is inversely related to the duration of $R(t)$ in the time domain, the integral of the truncated $|CBF \cdot R(f)|$ was used as this $MTT_{ESTIMATE}$ value. The magnitude operation is used to eliminate arterial tissue delay (ATD) effects on the estimator. The $MTT_{ESTIMATE}$ metric is robustly demonstrated in the "Results" section both in simulation and in patient data.

By making the extrapolation length inversely proportional to the $MTT_{ESTIMATE}$ value, correction for missing high-frequency components is achieved. To estimate the filtered (or thresholded) high-frequency signal components, simple extrapolation over a length,

$$L_{EXTRAPOLATE} = \frac{\chi}{MTT_{ESTIMATE}} \quad (7)$$

is performed in the frequency domain, where χ is a proportionality constant that will be derived empirically from simulations. Large extrapolation lengths required Fourier interpolation as the extrapolation lengths were greater than half the sampling frequency (extrapolated frequencies could be at orders much higher than what is sampled). During the extrapolation process, estimates on these frequency components are achieved.

With the missing high-frequency components corrected, the discrete time-domain signal will become much sharper, making it difficult to correctly identify its peak value from which CBF is estimated. To overcome this problem, the time-domain signal needs to be interpolated. This is straightforward to perform in the frequency domain using Fourier interpolation. The $R(f)$ frequency components after $L_{EXTRAPOLATE}$ where set to zero up to a length 4 N. After performing the inverse discrete Fourier transform (DFT), the residue function will be interpolated fourfold, allowing accurate estimates of the peak value, CBF, to be made.

3. Methods

3.1. Computer simulations

Simulations are undertaken to find optimal deconvolution parameters, the values used in simulation mimic parameters

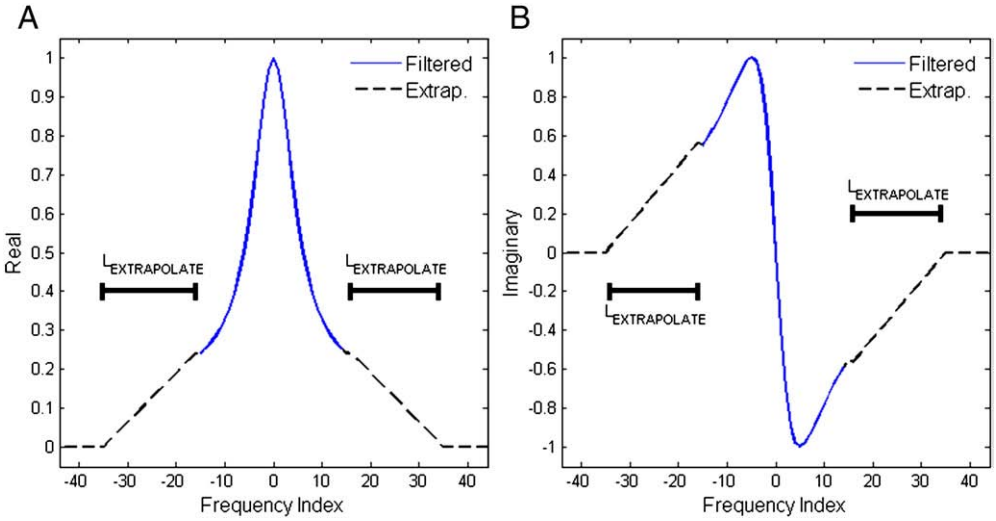

Fig. 2. Extrapolation of truncated signals. Extrapolation of the residue function is performed on both the real (A) and the imaginary (B) components of the residue function. The solid blue lines represent the signal after it has been truncated, and the dashed black lines represent the extrapolation of the signal as it is drawn out to a length of $L_{EXTRAPOLATE}$. Both of these signals are normalized. The key parameters used in the creation of the simulation were as follows: CBF=60 ml/100 g/min; CBV=5 ml/100 g; P_{SVD}=0.2; $L_{EXTRAPOLATE}$=20 pts; MTT=4 s; Δt=2 s.

of the current perfusion imaging protocol at our centre (described more thoroughly in the "Patient data" section). Concentration time signals are modeled using conventional estimates described in literature. The arterial input function, $C_a(t)$, was modeled by a normalized gamma-variate function,

$$C_a(t) = \begin{cases} \dfrac{C_{max}(t-T_A)^{\rho} e^{-(t-T_A)/\upsilon}}{(\rho)^{\upsilon} e^{\rho}} & t > T_A \\ 0 & \ldots \end{cases}, \quad (8)$$

with ρ set to 1.5 and υ set to 3 s^{-1} [6,12] and T_A being the arrival time of the contrast agent. The residue function, $R(t)$, was modeled using the single compartmental approximation,

$$R(t) = \begin{cases} e^{-\dfrac{t-\mathrm{ATD}}{\mathrm{MTT}}} & t > \mathrm{ATD} \\ 0 & \ldots \end{cases}, \quad (9)$$

where MTT is the MTT of bolus passing through the tissue.

Noise was introduced by first converting the simulated concentration time functions to MR signal intensity functions via Eq. 2 and adding Gaussian distributed random noise. The SNR_C was defined as $SNR_C = S_0/\sigma_{SIGNAL}$, where S_0 is the baseline signal, and σ_{SIGNAL} is the variance of the added noise.

Deconvolution was performed using the simulated noise-free and noisy $C_a(t)$ and $C_T(t)$ signals, and CBF was determined from the peak of the estimated deconvolved flow-scaled residue function. A variety of published MR perfusion deconvolution algorithms (SD, bcSVD, TikhoSVD and Tikhonov method) were used as benchmarks to compare against deconvolution with simple extrapolation.

Optimal filtering/thresholding parameters were determined by minimizing the CBF error across a range of MTT values. Each of the time-domain deconvolution methods has a parameter (either P_{SVD} or α) that first needed to be optimized versus SNR_C (ranging from 0 to 50). Similarly, the post-SD filter cutoff frequency (cf., Eq 7) was likewise optimized. The measured CBF was compared with the true expected CBF known from the simulation model description to obtain a relative error, $(CBF_{measured} - CBF_{true})/CBF_{true}$. The optimal filtering/threshold parameters were found by minimizing the root mean square (rms) error (Δ_{rms}) of the CBF values over a realistic physiological and pathophysiological range of MTT values (3 s<MTT<12 s).

To identify key features of and further refine the SD followed by simple extrapolation method, simulations were performed to validate the $MTT_{ESTIMATE}$ parameter and to determine the optimal value of χ. The $MTT_{ESTIMATE}$ value was calculated over a larger range of MTT values (2 s<MTT<20 s) and compared with the known MTT. The $MTT_{ESTIMATE}$ was calculated for CBV values of 5.00 ml 100 g^{-1} and 1.74 ml 100 g^{-1}, simulating gray matter (GM) and white matter (WM), respectively.

The simple extrapolation method was implemented; after SD, the resulting $CBF \cdot R(f)$ signal was padded with zeros from $L_{EXTRAPOLATE}$ to 4096 points to provide increased time resolution after the inverse DFT was performed. The optimal value for the extrapolation constant, χ, was found for each P_{SVD}, by again finding the value that minimized Δ_{rms} across a range of MTT (3 s<MTT<12 s). The optimal constant (χ_{OPT}) was then set to the value where Δ_{rms} was minimized for a given SD P_{SVD} and, hence, SNR_C.

3.2. Patient data

Ten acute ischemic stroke patient data sets were collected on a 3-T MR scanner (Signa VH/*i*; General Electric Healthcare, Waukesha, WI, USA). Informed written consent using an institutional review board-approved procedure was

obtained from all patients prior to imaging. As part of our clinical acute stroke imaging protocol, DSC T_2*-weighted perfusion images were collected. Full brain coverage was achieved with 17 contiguous gradient-recalled echo planar image slices, each 5 mm thick. The slices were obliquely oriented (para-axially), and data were acquired with a repetition time (TR)/echo time (TE)/flip were 2000 ms/30 ms/45°. The acquisition matrix was 144×144 over a 24-cm field of view, and the reconstructed images were interpolated to 256×256 with sinc interpolation. An 8-channel phased-array head coil was used, and the images from each channel were combined with the sum-of-squares method. Typically, an injection of 20 ml of 0.5 mmol ml^{-1} contrast agent (Magnevist, Berlex Canada, Pointe-Claire, QC, Canada) was injected with a power injector (Spectris; Medrad, Warrendale, PA, USA) at a rate of 5 ml s^{-1} intravenously and was followed by an injection of >20 ml of saline at the same rate. Total scan time was 100 s.

In-house software (written in Matlab, R2010a; The Mathworks, Inc., Natick, MA, USA) was used to process the patient data. MR signal intensity versus time functions were used to determine peak concentration and TTP maps. From these maps, an arterial input function, $C_a(t)$, was selected from the middle cerebral artery. This signal was chosen based on the anatomical position and characteristics of the signal (i.e., the selected signal was chosen to resemble the approximated gamma-variate distribution). The MR signal functions were extracted and converted to concentration time functions using Eq. (2).

To ensure that the $MTT_{ESTIMATE}$ values were indeed accurate in vivo, two relative MTT maps were produced from each image data set. The first MTT map was created using the calculated $MTT_{ESTIMATE}$ values, and the second map was produced via the central volume theorem (i.e., MTT=CBV/CBF). The SD deconvolution method was used to generate the CBF estimate. CBF maps were then created for each of the deconvolution methods (SD, bcSVD, TikhoSVD and the Tikhonov ridge regularization) for all 10 patient data sets. The SNR_C was determined, and the optimal parameters (α, P_{SVD} and χ, chosen as applicable) from each method were used in the deconvolution process.

Regions of interest were placed in the same spatial location across all the CBF map types in both healthy and ischemic GM and WM to measure the contrast. The stroke-affected regions were identified from the TTP maps (generally regions with greater than 2-s delay in contrast arrival), as this map showed good conspicuity of the ischemic areas and did not require deconvolution. The mean and standard deviations were computed for each region of interest in each CBF map across all the patients. CBF map image contrast was then calculated for both GM and WM by

$$\text{Image contrast} = \frac{|\text{CBF}_{\text{HEALTHY}} - \text{CBF}_{\text{ISCHEMIC}}|}{\text{CBF}_{\text{HEALTHY}} + \text{CBF}_{\text{ISCHEMIC}}}. \quad (10)$$

Image contrast from each of the CBF map types was compared against the simple extrapolation method using a two-way repeated-measures analysis of variance (ANOVA) test with the following factors: tissue type (WM or GM) and tissue state (normally perfused or ischemic) and interaction between tissue type and state, with a confidence level of $P<.05$ as significant. Post hoc ANOVA tests with Bonferroni correction were performed to find statistically significant differences versus the simple extrapolation approach.

Data were available for one patient who was not treated because he/she arrived past the window for thrombolytic intervention, thus allowing assessment of the natural course of the stroke. This patient was rescanned again after 30 days during a clinical follow-up study. For this patient, the initial scans (at stroke onset) showed a small abnormality on DWI, indicating a small core infarct volume. The follow-up fluid-attenuated inversion recovery (FLAIR) scan showed that the infarct had grown. The untreated patient provided an interesting opportunity to selectively test the perfusion–diffusion mismatch theory [4] and generate an ROC curve for distinguishing 30-day infarct from normal tissue as a function of baseline perfusion values. The images from the follow-up FLAIR study were spatially registered to the initial images. The pixels of the final infract on the FLAIR images were then identified. A changing CBF threshold was then applied across each of the CBF maps to determine the sensitivity versus 1 − specificity of detecting the final infarct.

4. Results

4.1. Computer simulations

The optimal filter cutoff/threshold parameter values for the four deconvolution techniques examined were plotted against SNR (Fig. 3). These values of P_{SVD} and α resulted in

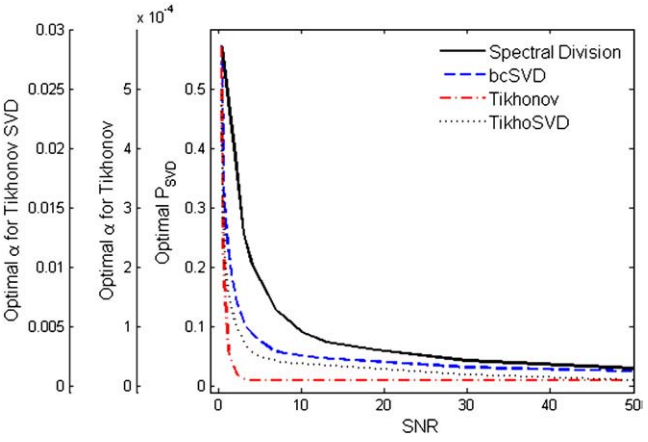

Fig. 3. Optimal deconvolution parameters that minimize the rms error in CBF as a function of SNR. Optimization of α and P_{SVD} parameters for the SD, bcSVD, TikhoSVD and Tikhonov methods for different levels of SNR. The frequency cutoff used for the low-pass filter in SD is related to P_{SVD} by Eq. 7. Parameters used in the simulations are as follows: CBF=60 ml/100 g/min; CBV=5 ml/100 g; MTT=4 s; Δt=2 s.

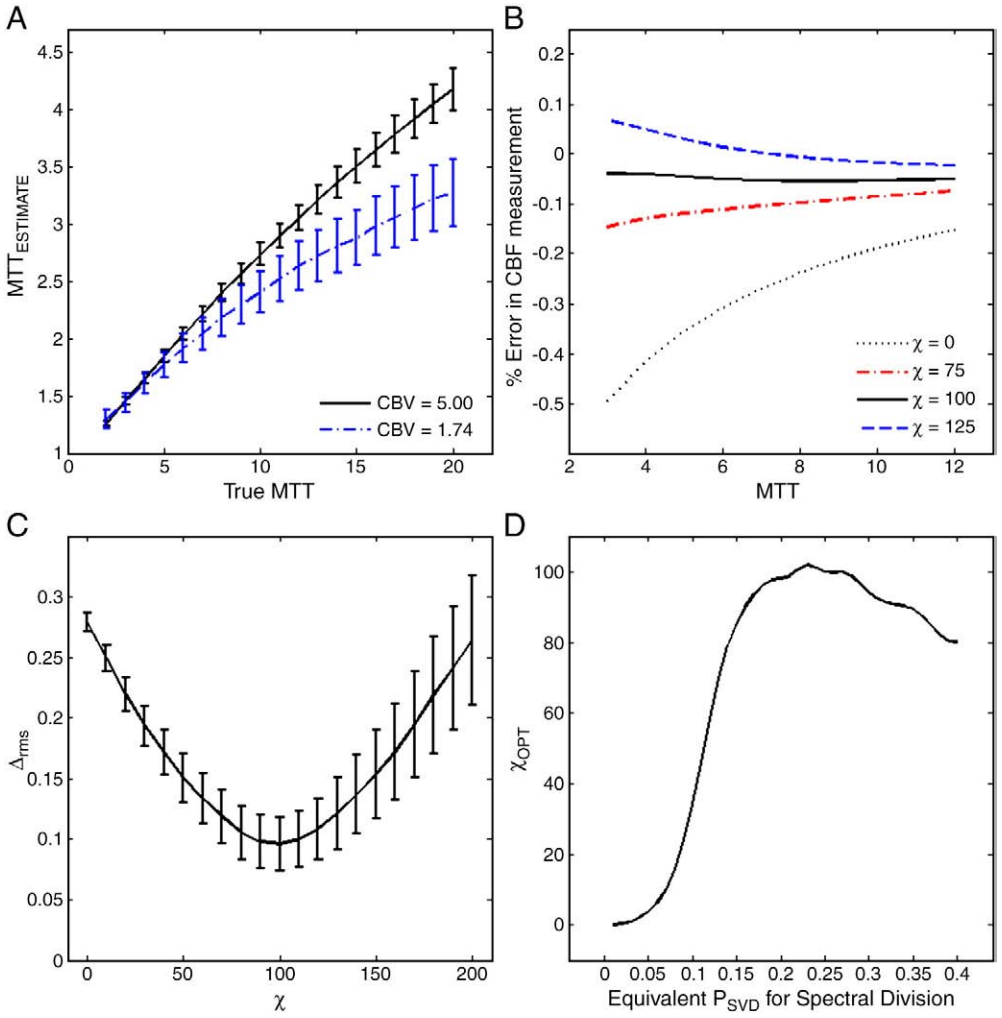

Fig. 4. (A) Using a Monte-Carlo simulation, the MTT was varied from 2 to 20 s. At each MTT in the simulation, the $MTT_{ESTIMATE}$ value was calculated using the procedure described in the text. The simulation shows a very linear response with a tight variance in the estimator for an SNR of 3 at small MTT. Simulation parameters were as follows: 1000 trials were run for each point, CBV=5.00 and 1.74 ml/100 g; ATD=0.17 s; P_{SVD}=0.2; Δt=2 s. (B) The effect of changing the extrapolation constant on CBF error versus MTT. A near-flat response can be achieved with an extrapolation constant of 100 at a P_{SVD} of 0.2. This result suggests that there is an optimal extrapolation constant (χ_{OPT}) that can be chosen to minimize the error. (C) Monte-Carlo simulations were again undertaken, this time to find χ_{OPT} for a PSVD of 0.2 at an SNR=3. It was found that χ_{OPT} constant did not change greatly with SNR, if the appropriate PSVD was chosen. (D) χ_{OPT} did change with the PSVD, and the Monte-Carlo simulation was varied to find the best choice of χ_0, given PSVD.

the smallest error (Δ_{rms}) and, thus, the least degree of MTT dependence for a given SNR_C.

For low SNR studies, The $MTT_{ESTIMATE}$ simulations (Fig. 4A) had good linearity and were monatomic. The data obtained for lower CBV were less linear over the evaluated range of MTT. The estimator also had a small variance for small MTT, even given the poor SNR (SNR=3 in this example). The observed variance changed with MTT, suggesting that there will be an increase in the noise of the $MTT_{ESTIMATE}$ maps for increasing MTT. These $MTT_{ESTIMATE}$ results are likely acceptable for our purposes, because the extrapolation length will be largest and have the greatest impact at short MTT (Eq. 7), and this is the region where $MTT_{ESTIMATE}$ is most linear and has the lowest variance.

Application of simple extrapolation was able to change the extent of the MTT-dependant response (Fig. 4B), and an optimal extrapolation constant (where the CBF error vs. MTT curve was fat and close to no error) could be determined. When the extrapolation constant is plotted against the rms error (Δ_{rms}), there is a clear minima (Fig. 4C). In the example case of SD deconvolution at an equivalent P_{SVD} of 0.2, the extrapolation constant yielding the smallest Δ_{rms} was χ=100. Additional simulations were undertaken at different SNR_C, and it was determined that if the P_{SVD} used for SD was chosen appropriately, then this removed the SNR dependence on the optimal χ (i.e., changes in SNR did not change the optimal value of χ). For example, in the case of SD (Fig. 4D), setting P_{SVD}>0.15 produced nearly constant results for χ,

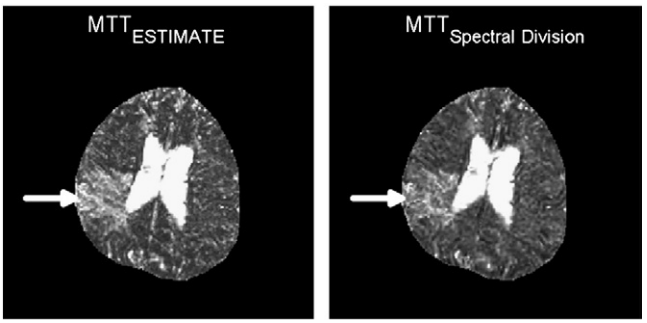

Fig. 5. Comparison of $MTT_{ESTIMATE}$ map (left) and a conventional MTT map produced with windowed SD deconvolution (right). There is a region of reduced blood flow and increased MTT (arrows). This region is, in general, comparable between the two maps. There appears to be an increase in noise in the normal tissue regions of the MTT estimator map; an increase in variance is expected from the results of the simulation Fig. 4A. We would expect to find a larger increase in variance in the longer MTT region as well. Note that CSF is given a higher MTT value in the MTT estimator map than the conventional estimate; this will result in a lower extrapolation length value in the extrapolated CBF maps, which is desirable.

suggesting that the optimal extrapolation constant was nearly independent of P_{SVD} value.

4.2. Patient data

A representative $MTT_{ESTIMATE}$ map is displayed along with a conventional MTT map (Fig. 5). The region of increased MTT was clearly defined on both images. There was an observed increase in the noise of the MTT estimates, and this increase was particularly evident in healthy tissues, as was expected from simulations (Fig. 4A). While not as apparent, there was also an increase in the variance in tissues with longer MTT (i.e., within the lesion region). While the estimated MTT map was noisier, as expected, it tracked the true MTT values and thus was suitable for our application. The $MTT_{ESTIMATE}$ map provided a readily calculated approximation of the conventional MTT map.

Averaged results from each deconvolution method (image contrast in the CBF maps) across the 10 patient data sets are shown in Table 1. The simple extrapolation method showed a mean increase in image contrast compared with all other methods of between 125% and 266%. Statistical significant differences in CBF image contrast were found when comparing simple extrapolation against all of the methods. ANOVA testing showed that the CBF image contrast was significantly affected (F=4.73, P=.001) by deconvolution method (F=9.40, P=.001) but not by tissue type (F=1.41, P=.2379) or the deconvolution method-tissue type interaction (F=0.88, P=.4792). The post hoc comparisons showed that simple extrapolation was statistically different (P<.05) in both tissue types, except when comparing GM with the TikhoSVD method (P=1.000) and the Tikhonov method (P=.417) and when comparing WM with the TikhoSVD method (P=.108).

An example series of CBF maps of an untreated patient are shown along with initial DWI and 30-day follow-up FLAIR images (Fig. 6). Each of the perfusion deconvolution methods shows a lesion on the CBF map that corresponds to follow-up imaging. However, there is a varying degree to which these lesions are visible and match the 30-day lesion. The bcSVD and SD deconvolution methods, for example, do not show the same conspicuity of the ischemic lesion compared with the other methods. The simple extrapolation method best matched the 30-day outcome lesion. The ROC curve (Fig. 7) derived from the data in Fig. 6 also demonstrated that simple extrapolation performed the best. The TikhoSVD method also performed well, followed by the SD and Tikhonov methods. The bcSVD method had the worst performance in this patient.

5. Discussion

The results show an increase in image contrast between healthy and ischemic tissues when using the simple extrapolation technique when compared with other deconvolution methods. Regions that are likely to become core infarct are more conspicuous on CBF maps reconstructed with the simple extrapolation during early ischemic events. Patient data matched simulation results; as expected there, was a relative increase of CBF values in normally perfused tissues using simple extrapolation, while tissues that were ischemic and had longer MTT values were not as affected. By estimating MTT prior to deconvolution, the error in CBF for

Table 1
Normal and ischemic tissue image contrast in CBF maps averaged over 10 patients

Method	Measured image contrast		Comparison vs. simple extrapolation		% Increase in CBF image contrast	
	GM	WM	GM	WM	GM	WM
Simple extrapolation	0.5144±0.1280	0.5057±0.1715	NA	NA	NA	NA
SD	0.2505±0.1493	0.2550±0.1511	P=.001	P=.026	205%	198%
bcSVD	0.1931±0.1425	0.2282±0.1514	P=.001	P=.010	266%	222%
TikhoSVD	0.4104±0.1976	0.2968±0.1947	P=1.000	P=.108	125%	170%
Tikhonov	0.3620±0.1847	0.2436±0.2030	P=.417	P=.017	142%	208%

All other methods are compared against the simple extrapolation method with two-way repeated-measures ANOVA comparison tests. ANOVA testing showed that the CBF image contrast was significantly affected (F=4.73, P=.001) by deconvolution method (F=9.40, P=.001) but not by tissue type (F=1.41, P=.2379) or the deconvolution method-tissue type interaction (F=0.88, P=.4792).

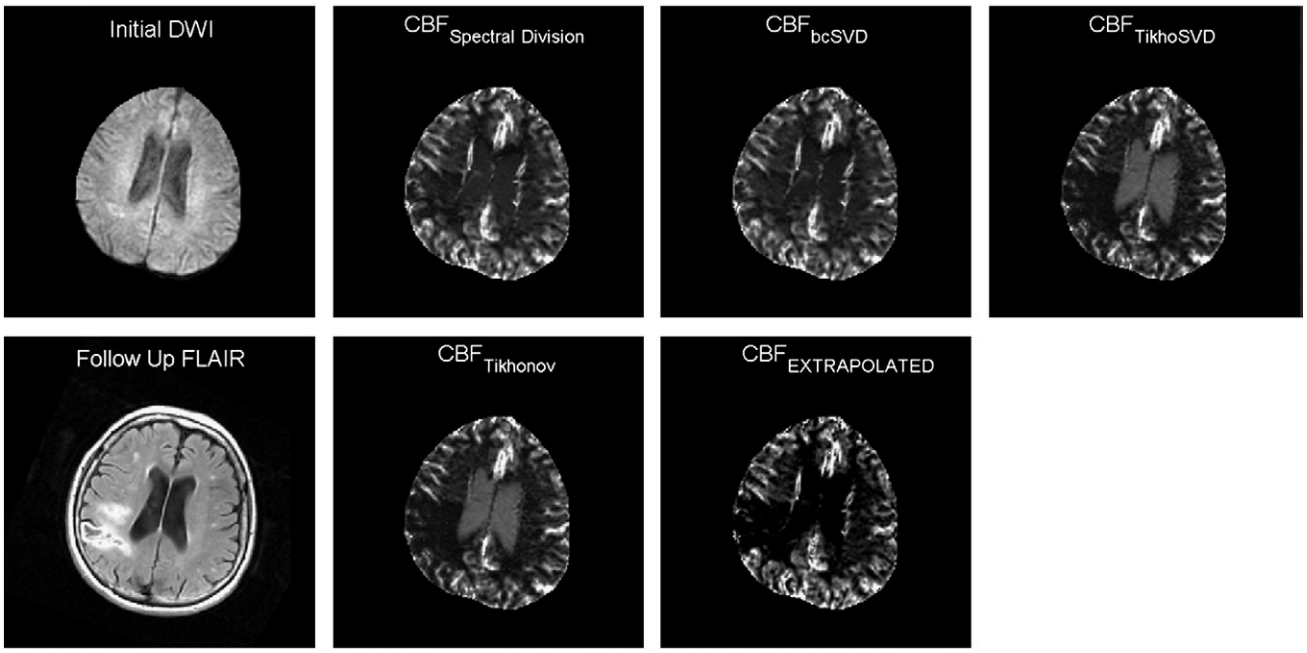

Fig. 6. Initial and follow-up imaging for untreated acute ischemic stroke patient (top left) shows initial DWI image with a small infarct in the ischemic region (bottom left). FLAIR imaging that took place 30 days after the stroke. Follow-up image was registered to perfusion images at onset. The core infarct has grown significantly. According to the diffusion–perfusion mismatch theory, we would anticipate that the CBF map would show us this final infarct region during the initial imaging procedure. All five methods for generating CBF maps are shown here. These methods have varying degrees of lesion definition and correspondence to outcome by 30-day FLAIR imaging.

normal (short MTT) signals was minimized. The resulting increase in CBF values for healthy tissue increased the image contrast observed between normal and ischemic regions.

The computational requirements of each method should be considered when implementing deconvolution techniques. Data were processed using commercial numerical simulation software (R2010a; The Mathworks, Inc.), and

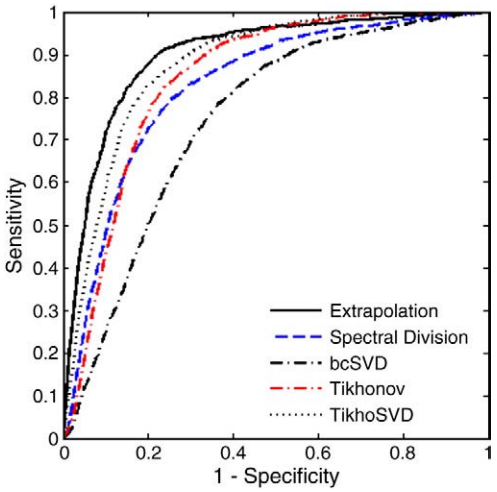

Fig. 7. ROC curve for detection of final infarct using the five CBF maps is shown. The final infarct was determined from the infarct on the 30-day follow-up FLAIR image. Only pixels containing GM and/or WM were used in this analysis. The extrapolated CBF map was the best technique for detection of the penumbral region in this patient example.

total processing time was not directly addressed in the results presented; however, the time required for each of the methods is relevant in acute ischemic stroke when implementing and clinically using any of these techniques. All processing was performed in a multithreading environment; all of the algorithms could be accelerated with increased data pipelines. All of the SVD-based and the Tikhonov ridge techniques were processed in approximately the same period of time on the order of 20 s per PWI data set. They all ran in approximately the same period of time because most of the computational time was required for matrix multiplications, and the time required to invert the $\boldsymbol{C}_a$ matrix was relatively short. The SD method required approximately twice the time of the SVD methods. The simple extrapolation method was the most computationally intensive and took almost three times longer than the SD method, requiring almost 2 minutes per data set. Implementation of the methods in C/C++ would likely reduce these computation periods drastically.

The extrapolation process was very quick, but this implementation required Fourier interpolation, which increased the total processing duration. Selection of a shorter interpolation length would be recommended. Our experience suggests that DFT transformations on the order of 256 points would be as effective as the method used in this study (interpolation to 4096 points). Interpolating to this shorter length would result in a shorter processing time while still allowing for sufficient extrapolation lengths. In our patient studies, the maximum extrapolation length for normal tissues was $\leq$140 points.

This work showed improved accuracy in CBF perfusion images when simple extrapolation was used. Simple extrapolation is a linear approach and maintains first-order continuity in the frequency domain (i.e., there are no discontinuities in the frequency-domain signal). Simple extrapolation can be used with other deconvolution approaches. In principle, more sophisticated extrapolation techniques such as higher order extrapolation and auto regressive moving average techniques [21–23], which maintain higher orders of signal continuity, would be preferred [24]. However, due to MR perfusion acquisition limitations, few nonzeroed data points are generally available; these more sophisticated techniques tend to be, in practice, less effective. Model-based filtering may also be beneficial when dealing with multiple residue function types (i.e., biexponential model types used for permeability measurements). However, for this study, we used the simplest and most widely accepted technique, an exponential decay function. The performance of the simple extrapolation method on patient data confirms a degree of independence of the method on the chosen residue function model. More adaptive filtering-based techniques could also be effective in improving image contrast, although we would hypothesis that such techniques would still benefit from frequency-domain extrapolation, such as the simple extrapolation approach presented here.

Acknowledgements

The authors would like to thank the Canadian Institutes for Health Research and National Science and Engineering Research Council of Canada (NSERC) for their financial support. The authors would also like to thank Jayme C Koisor, PhD; Juan Quan, MSc; Marina Salluzzi, PhD; and Julia Stanley, MSc, for their assistance. M.E.M. was an NSERC Undergraduate Student Research Award holder and is currently an NSERC Graduate Scholarship holder. M.R.S. is an Analog Devices University Ambassador. R.F. is a Canada Research Chair in Image Science and the Hopewell Professor of Brain Imaging and was an Alberta Heritage Foundation for Medical Research Senior Scholar.

References

[1] Easton JD, Saver JL, Albers GW, Alberts MJ, Chaturvedi S, Feldmann E, et al. Definition and evaluation of transient ischemic attack. Stroke 2009;40:2276–93.
[2] Sacco RL, Adams R, Albers G, Alberts MJ, Benavente O, Furie K, et al. Guidelines for prevention of stroke in patients with ischemic stroke or transient ischemic attack. Stroke 2006;37:577–617.
[3] Lauzon ML, Sevick RJ, Demchuk AM, Frayne R. Stroke imaging at 3.0 T. Neuroimaging Clin N Am 2006;16:343–66.
[4] Neumann-Haefelin T, Wittsack HJ, Wenserski F, Siebler M, Seitz RJ, Modder U, et al. Diffusion- and perfusion-weighted MRI: the DWI/PWI mismatch region in acute stroke. Stroke 1999;30:1591–7.
[5] Müller TB, Haraldseth O, Jones RA, Sebastiani G, Godtliebsen F, Lindboe CF, et al. Combined perfusion and diffusion-weighted magnetic resonance imaging in a rat model of reversible middle cerebral artery occlusion. Stroke 1995;26:457–8.
[6] Østergaard L, Weisskoff RM, Chesler DA, Gyldensted C, Rosen BR. High resolution measurement of cerebral blood flow using intravascular tracer bolus passages. Part I: mathematical approach and statistical analysis. Magn Reson Med 1996;36:715–25.
[7] Østergaard L, Sorensen AG, Kwong KK, Weisskoff RM, Gyldensted C, Rosen BR. High resolution measurement of cerebral blood flow using intravascular tracer bolus passages. Part 2: experimental comparison and preliminary results. Magn Reson Med 1996;36:726–36.
[8] Salluzzi M, Frayne R, Smith MR. An alternative viewpoint of the similarities and differences of SVD and FT deconvolution algorithms used for quantitative MR perfusion studies. Magn Reson Imaging 2005 (23):481–92.
[9] Kosior JC, Frayne R. PerfTool: a software platform for investigating bolus-tracking perfusion imaging quantification strategies. J Magn Resonance Imaging 2007(25):653–9.
[10] Calamante F, Gadian DG, Connelly A. Delay and dispersion effects in dynamic susceptibility contrast MRI: Simulations using singular value decomposition. Magn Reson Med 2000;44(3):466–73.
[11] Smith MR, Lu H, Trochet S, Frayne R. Removing CBF artifacts introduced during SVD deconvolution. Proc. 11th ISMRM, 2003. p. 2206.
[12] Liu HL, Pu Y, Liu Y, Nickerson L, Andrews T, Fox PT, et al. Cerebral blood flow measurement by dynamic contrast MRI using singular value decomposition with an adaptive threshold. Magn Reson Med 1999;42(1):167–72.
[13] Larsson HBW, Courivaud F, Rostrup E, Hansen AE. Measurement of brain perfusion, blood volume, and blood–brain barrier permeability, using dynamic contrast-enhanced T1-weighted MRI at 3 tesla. Magn Reson Med 2009;62(5):1270–81.
[14] Chen JJ, Smith MR, Frayne R. Advantages of frequency-domain modeling in dynamic-susceptibility contrast magnetic resonance cerebral blood flow quantification. Magn Reson Med 2005;53(3):700–7.
[15] H Lu MS, Frayne R. Quantitative MR cerebral blood flow using ARMA-based deconvolution: preliminary results. IEEE 2002:1171–6.
[16] Sourbron S, Luypaert R, Schuerbeek PV, Dujardin M, Stadnik T, Osteaux M. Deconvolution of dynamic contrast-enhanced MRI data by linear inversion: choice of the regularization parameter. Magn Reson Med 2004;52(1):209–13.
[17] Chen JJ, Frayne R, Smith MR. Reassessing the clinical efficacy of two MR quantitative DSC PWI CBF algorithms following cross-calibration with PET images. Physics in Medicine and Biology 2005;50(6):1251.
[18] Wu O, Østergaard L, Weisskoff RM, Benner T, Rosen BR, Sorensen AG. Tracer arrival timing-insensitive technique for estimating flow in MR perfusion-weighted imaging using singular value decomposition with a block-circulant deconvolution matrix. Magn Reson Med 2003;50(1):164–74.
[19] Smith MR, Lu H, Trochet S, Frayne R. Removing the effect of SVD algorithmic artifacts present in quantitative MR perfusion studies. Magn Reson Med 2004(51):631–4.
[20] Hansen C. Rank-deficient and discrete ill-posed problems: numerical aspects of linear inversion. Philadelphia: Society of Industrial and Applied Mathematics; 1997.
[21] Smith MR, Lu H, Frayne R. Signal-to-noise ratio effects in quantitative cerebral perfusion using dynamic susceptibility contrast agents. Magn Reson Med 2003;49:122–8.
[22] Smith MR, Nichols ST, Henkelman RM. Application of autoregressive moving average parametric modeling in magnetic resonance image reconstruction. IEEE Transactions on Medical Imaging 1986;5(3): 132–9.
[23] Salluzzi M, MRS, Frayne R. Applying the transient error reconstruction algorithm in the assessment of the cerebral blood flow. 26th Annual International Conference of the IEEE Engineering in Medicine and Biology Society, September 2004, San Francisco, CA, USA; 2004. p. 1092–5.
[24] Harris FJ. On the use of windows for harmonic analysis with the discrete Fourier transform. Proceedings of the IEEE 1978;66(1): 51–83.